Talanta 218 (2020) 121126

Contents lists available at ScienceDirect

Talanta

journal homepage: www.elsevier.com/locate/talanta

A novel label-free solid-state electrochemiluminescence sensor based on the resonance energy transfer from $Ru(bpy)_3^{2+}$ to GO for DNA hybridization detection

Baomei Huang[a,*], Chengwei Yao[b], Yunju Zhang[a], Xiaoquan Lu[c]

[a] College of Chemistry & Chemical Engineering, MianYang Normal University, MianYang, 621000, China
[b] Facility Design and Instrumentation Institute, China Aerodynamics Research and Development Center, MianYang, 621000, China
[c] Key Laboratory of Bioelectrochemistry & Environmental Analysis of GansuProvince, College of Chemistry & Chemical Engineering, Northwest Normal University, Lanzhou, 730070, China

ARTICLE INFO

Keywords:
Solid-state electrochemiluminescence
Ruthenium
Graphene oxide
Resonance energy transfer
DNA

ABSTRACT

Based on electrochemiluminescence resonance energy transfer (ERET) from $Ru(bpy)_3^{2+}$ to graphene oxide (GO), a novel label-free solid-state ECL sensor for sensitive detection of DNA was proposed. First, $Ru(bpy)_3^{2+}$/AuNPs was successfully prepared by using a simple and green method and characterized by transmission electron microscopy (TEM), Energy Dispersive X-ray (EDX), and UV–vis spectroscopy. Then, the $Ru(bpy)_3^{2+}$/AuNPs colloid was assembled on the gold electrode surface for solid-state ECL film which also later could be used to immobilize thiol-derivatized, single-stranded DNA (HS-ssDNA) via Au–S interactions. The stepwise modification procedure was characterized by cyclic voltammetry(CV), electrochemical impedance spectroscopy (EIS), probe approach curves (PAC) and ECL, respectively. The resulting modified electrode was tested as ECL biosensor for DNA detection. Upon addition of GO, the strong noncovalent interaction between HS-ssDNA and GO led to ECL quenching because of ERET. When in the presence of target ssDNA (t-ssDNA), the distance between the HS-ssDNA and GO increased, which significantly hindered the ERET and, thus, resulted in the restoration of ECL. The ECL intensity of the biosensor increased linearly with t-ssDNA concentration in the range of 50–1000pM, and the detection limit is 20pM. To the best of our knowledge, this is the first application of solid-state ERET from $Ru(bpy)_3^{2+}$ to GO and opens new opportunities for sensitive detection of biorecognition events.

1. Introduction

As the human genome project has uncovered the full sequence of human genomes and the postgenome technologies have been rapidly developed, DNA hybridization detection has become increasingly important [1]. DNA hybridization detection can be through changes in mass [2], optical properties [3–5], electrochemical properties [6–10], surface plasmon resonance (SPR) [11,12] or electrochemiluminescence (ECL) [13–16].

Among various biosensing technologies, ECL hold great promise since it could combine the advantages of both electrochemical and chemiluminescent, such as strong signal response, inherent sensitivity, simplified optical setup and low background signal. $Ru(bpy)_3^{2+}$(or its derivatives) with TPA exhibit the highest ECL efficiency, so this system has been widely utilized in a number of bioanalytical areas, such as immunoassays, DNA analyses et al. [17–23]. However, many of these applications require prior labeling of the DNA target or probe with Ru $(bpy)_3^{2+}$ which make the experiments relatively complex, time-consuming and might affect the bioaffinity of recognition element for its cognate target.

Solid-state ECL can reduce the consumption of expensive reagent, enhance the ECL signal, simplify experimental design and create regenerable label-free sensors. Thus, the immobilization of $Ru(bpy)_3^{2+}$ on electrode surface is of great interest. many methods of achieving this have been reported [24]. A popular method is the incorporation of Ru $(bpy)_3^{2+}$ in Nafion since its ion-exchange selectivity coefficients for Ru $(bpy)_3^{2+}$ is as high as 5.7×10^6. However, the structure of Nafion made the immobilized $Ru(bpy)_3^{2+}$ likely partition into the hydrophobic regions, thus resulting in charge transport difficulty within the film. The combination of the electronic conductivity and electroactivity properties of metal nanoparticles(NPs) allowed faster diffusion of the analytes into the film and accelerated charge transportation. For example, Wang and co-workers [25–27] have synthesized $Ru(bpy)_3^{2+}$/AuNPs(PtNPs) in aqueous solution, which was used for solid-state ECL biosensor

* Corresponding author.
E-mail address: hbm790117@163.com (B. Huang).

https://doi.org/10.1016/j.talanta.2020.121126
Received 18 March 2020; Received in revised form 30 April 2020; Accepted 4 May 2020
Available online 06 May 2020

material by other researchers [28–30]. Chen and co-workers [31] reported on the fabrication of a three dimensionally (3D) ordered macroporous gold film electrode as the matrix for efficient immobilization of $Ru(bpy)_3^{2+}$ in zirconia-Nafion sol-gel film. Although these obviously improved the stability of the sensor, the synthesis process was inconvenient or has low yield.

Graphene oxide (GO), a two-dimensional chemically modified graphene sheet [32], has attracted considerable attention in different fields due to its unique and interesting electronic, thermal and mechanical properties. As strong noncovalent binding of GO with nucleobases and aromatic compounds has been reported [33], it acts as a quencher to quench the fluorescence by strong interaction between ssDNA and GO [34–37]. However its application in ECL-based bioanalysis is rather limited. Liu's group [38] has proposed a sensing strategy for sensitive detection of mucin 1 protein (MUC1) and MCF-7 cells based on ERET from bis(2,2′-bipyridine)-(5- aminophenanthroline)ruthenium(II) to GO. But it was carried out in solution phase, which required prior labeling of DNA target or probe with ECL markers and more consumption of expensive reagent. To date, label-free ECL biosensors based on ERET from $Ru(bpy)_3^{2+}$ to GO have not been reported.

In this paper, first, $Ru(bpy)_3^{2+}$/AuNPs was successfully prepared by using a facile and green method which is quite stable and has excellent ECL behavior and wonderful bioconjunction. It was characterized by transmission electron microscopy (TEM), Energy Dispersive X-ray (EDX), and UV–vis spectroscopy. Then, directly coating the as-prepared colloid on the surface of gold electrode surface produces a solid-state ECL film which later was used to indirectly label HS-ssDNA because the DNA is closely attached onto the $Ru(bpy)_3^{2+}$/AuNPs composite V*ia* Au–S interaction. The stepwise modification procedure was characterized by cyclic voltammetry(CV), electrochemical impedance spectroscopy (EIS), probe approach curves (PAC) and ECL, respectively. The resulting modified electrode was tested as ECL biosensor for DNA detection. Upon addition of GO, due to the strong noncovalent interaction between the HS-ssDNA and GO, the ECL of $Ru(bpy)_3^{2+}$ was efficiently quenched because of ERET. In the presence of target ssDNA (t-ssDNA), the binding between the HS-ssDNA and t-ssDNA disturbed the interaction between the HS-ssDNA and GO, the distance between the HS-ssDNA and GO increased, which significantly hindered the ERET and, thus, resulted in the restoration of $Ru(bpy)_3^{2+}$ ECL (Scheme 1). This was shown to detect t-ssDNA sensitively in a linear range from 50 to 1000 pM with a detection limit of 20pM. The label-free approach was used to detect DNA with advantages such as less labor for synthesis of the $Ru(bpy)_3^{2+}$-based probe; reducing the consumption of expensive reagent; simplifying experimental design and having high stability and good specificity. Therefore, the simple solid-state $Ru(bpy)_3^{2+}$ ECL film is better than the other ECL quenching methods and can be utilized as reagentless DNA ECL biosensors.

2. Experimental section

2.1. Chemicals and apparatus

Oligonucleotides were purchased from Shenggong Bioengineering Ltd Company (Shanghai, China) and purified using high-performance liquid chromatography. The oligonucleotide sequences are shown as follows:

HS-ssDNA: 5′-GTG TGG TTG GAT TGA TCG TAG GTA – $(CH_2)_6$-SH -3'

perfectly complementary strand: 5′- TAC CTA CGA TCA ATC CAA CCA CAC -3'

single-base mismatch stand: 5′- TAC ***A***TA CGA TCA ATC CAA CCA CAC -3'

three-base mismatch stand: 5′- TAC ***A***TA CGA TCA ***G***TC CAA CC***T*** CAC -3'

non-complementary strand: 5′-ACT TAG ATT CAG CAT ACG AAT AGA–3'

Cyclic voltammogram(CV) and ECL experiments were performed using a model MPI-A electrochemiluminescence analyzer system (Xi'an Remax Electronic Science & Technology Co. Ltd., Xi'an, China). Atomic force microscopy (AFM) measurements were carried out at ambient temperatures with an Agilent 5400 AFM. UV–vis absorption spectra were taken by absorption mode with a UV-1102 UV–vis spectrophotometer (Shanghai, China). The infrared spectra(IR) were measured by FT-IR spectrometer (Bruker Vertex 70v). Raman spectra were obtained on J-Y T64000 Raman spectrometer. Transmission electron microscopy (TEM) measurements were made on a Hitachi H-8100 electron microscope (Hitachi, Tokyo, Japan). Electrochemical impedance spectroscopy (EIS) experiments were performed on Multi-potentiostat (VMP2, Princeton Applied Research, USA). Probe approach curves (PAC) were carried out using a CHI 900 scanning electrochemical microscope (CH Instruments Co. Ltd., Austin, TX) with a four-electrode cell. The gold (or modified gold) electrode, a platinum wire, and a KCl saturated Ag/AgCl electrode were used as the substrate, counter, and reference electrode, respectively. The SECM tip was a 12.5 μm diameter Pt ultramicroelectrode (UME).

2.2. Preparation of GO

Graphene oxide(GO)was prepared from natural graphite powder through a modified Hummers' method [39]. In a typical synthesis, 1 g of graphite was added into 23 mL of 98% H_2SO_4, followed by stirring at room temperature over a 24 h period. After that, 100 mg of $NaNO_3$ was introduced into the mixture and stirred for 30min. Subsequently, the mixture was kept below 5 °C by ice bath, and 3 g of $KMnO_4$ was slowly added into the mixture. After being heated to 35–40 °C, the mixture was stirred for another 30 min. After that, 46 mL of water was added into above mixture during a period of 25min. Finally, 140 mL of water and 10 mL of 30% H_2O_2 were added into the mixture to stop the reaction. After the unexploited graphite in the resulting mixture was removed by centrifugation, as-synthesized GO was dispersed into individual sheets in distilled water at a concentration of 0.5 mg mL^{-1} with the aid of ultrasound for further use.

2.3. Preparation of $Ru(bpy)_3^{2+}$/AuNPs

$Ru(bpy)_3^{2+}$/AuNPs colloid was prepared as follows. In a typical experiment, 20 μL of Nafion was diluted to 5 mL with water and 20 μL of 10 mM $Ru(bpy)_3^{2+}$ aqueous solution was added under stirring at room temperature. Then 100 μL of 24.28 mM $HAuCl_4$ was introduced into the resulting solution and the mixture was heated to 80 °C. After adding 1% $NaBH_4$ solution 40 μL, the as-formed solution was maintained at 80 °C for 20min, the black $Ru(bpy)_3^{2+}$/AuNPs colloid was prepared. The Nafion-stabilized Au nanoparticle (AuNPs/Nafion) colloid was prepared the same as the above procedure in the absence of $Ru(bpy)_3^{2+}$.

2.4. Fabrication of the solid-state ECL sensing platform

The surface of Au electrode was polished with an alumina slurry and rinsed with water and ethanol in an ultrasonic bath briefly. The Au electrode was further treated electrochemically in 0.5 M H_2SO_4 by scanning from −0.1 to 1.5 V at a scan rate of 100 mV s^{-1} for 15 min until an ideal voltammogram was observed. The 6 μL aliquot of $Ru(bpy)_3^{2+}$/AuNPs colloid was placed on the Au electrode surface. The as-prepared electrode was air-dried at room temperature in dark. After rinsing with water thoroughly, the solid-state ECL film was formed.

2.5. Immobilization of HS-ssDNA onto the solid-state ECL sensing platform

First, A 4 μL aliquot of 1 *n*M HS-ssDNA in 100 mM PBS(0.1 M KH_2PO_4 + 0.1 M K_2HPO_4 + 0.1 M KCl, pH7.4) was pipetted onto the surface of $Ru(bpy)_3^{2+}$/AuNPs/Au electrode as uniformly as possible

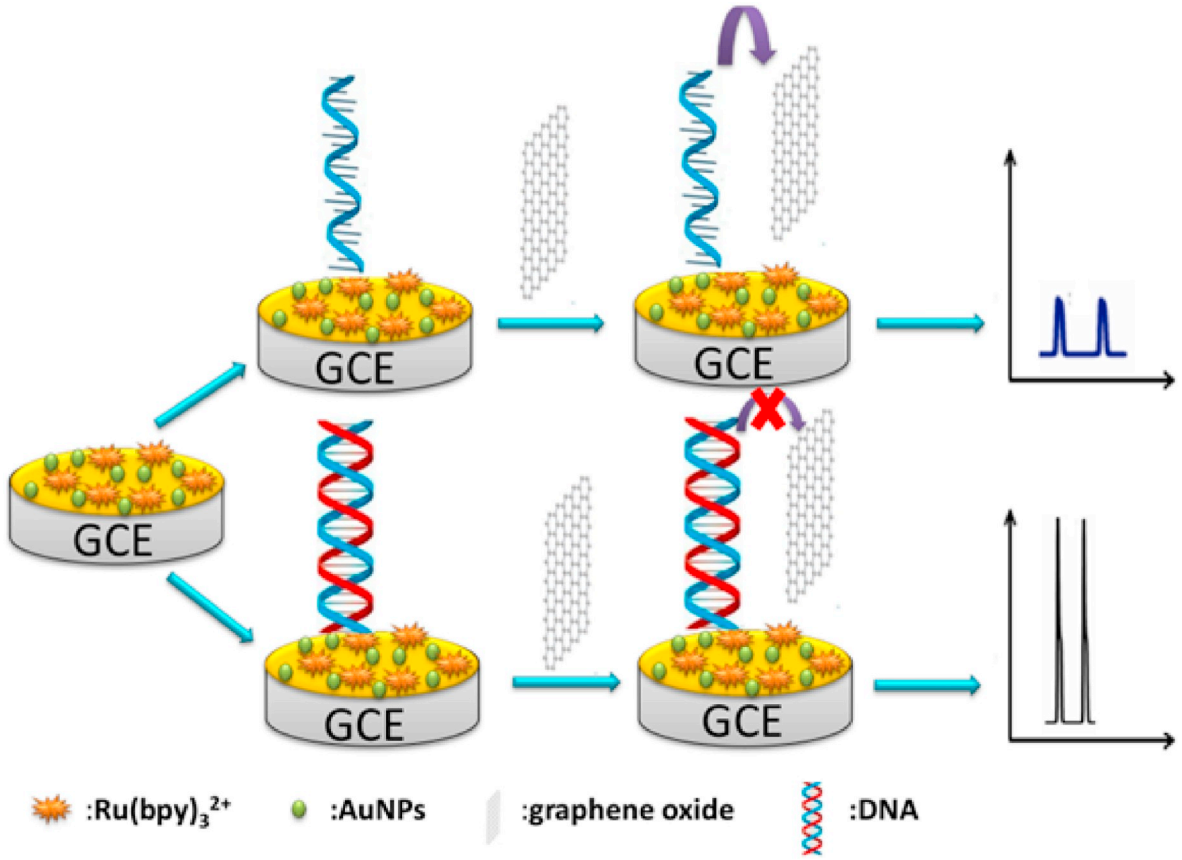

Scheme 1. Schematic representation of GO-induced solid-state ECL film quenching of Ru(bpy)$_3^{2+}$ and biosensing mechanism.

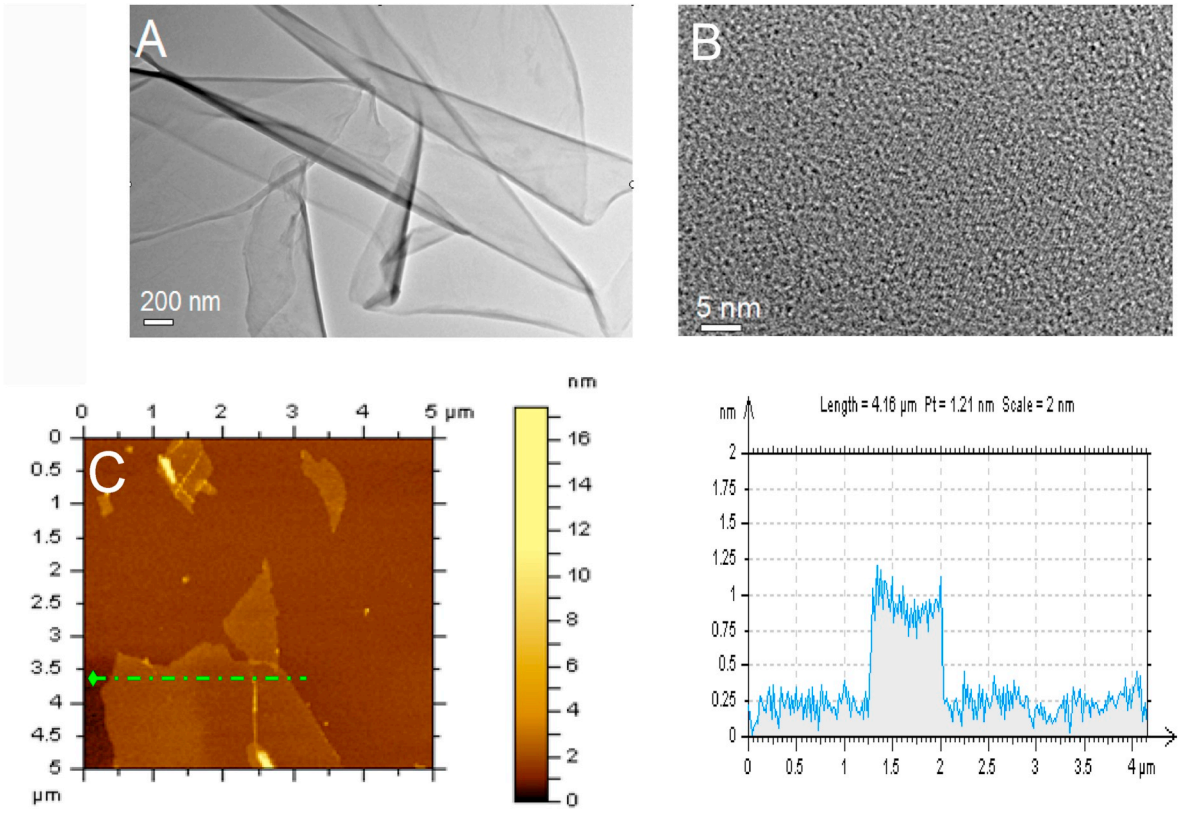

Fig. 1. TEM (A) and HRTEM(B) images of GO sheets and tapping mode AFM image of GO sheets deposited on mica substrate (C).

and self-assembled for 240 min at room temperature V*ia* Au–S interactions, followed by rinsing with PBS. Second, the HS-ssDNA-treated electrode was placed with 1.0 mM MCH for 2 h to adjust the distributing degree of the HS-ssDNA on the electrode. After rinsing with PBS thoroughly, HS-ssDNA was formed on the $Ru(bpy)_3^{2+}$/AuNPs/Au electrode surface.

2.6. DNA hybridization

The above modified electrode was immersed in 1.0 mL TE (10 mM Tris-HCl, 1 mM EDTA, 1 M NaCl, pH8.0) containing different concentrations of t-ssDNA at 37 °C for 90min to hybridize. Then, the hybridized electrode was rinsed with TE thoroughly to remove the unbinding DNA.

2.7. ECL detection

ECL with continuous potential scanning from 0.2 to 1.25 V and scanning rate of 100 mV s^{-1} was applied to achieve ECL signal in100mM PBS containing 3 mM TPA. A high voltage of 550 V was supplied to the photomultiplier to determine the ECL intensity. The ECL and CV curves were measured simultaneously. Before analysing, GO was incubated in the ECL detection cell for 5min.

3. Results and discussions

3.1. Characterization of GO

Fig. 1A shows the transmission electron micrograph (TEM) of GO with corrugated flakelike shapes. Mono-layer sheets could be observed in most of regions, whereas restacked parts and wrinkles could also be seen, which could be attributed to electronic repulsion between the soft and flexible layers. Fig. 1B shows a representative HRTEM image of GO, we can find the stacking sheet structure of GO in the TEM cross-sections, and individual layers of GO are clearly observed. From the cross-sectional view of the typical AFM image (Fig. 1C), the average thickness of GO sheet was about 0.8 nm thick. This observation is in agreement with previous AFM studies which objects to single-layer graphene oxide sheets [40–43]. The successful synthesis of GO was also demonstrated by UV, FT-IR, Raman spectra in the supplemental information(Figure S1, S2 and S3).

3.2. Characterization of $Ru(bpy)_3^{2+}$/AuNPs

Fig. 2A shows a TEM of the $Ru(bpy)_3^{2+}$/AuNPs. The dark spots and light features corresponded to AuNPs and the Nafion matrix, respectively. One can see that AuNPs were highly dispersed in the composite, and were small in size (~ 3 nm). Moreover such AuNPs were stable for several months without any observable aggregation, indicating that Nafion serves as a very effective dispersant for the formation of AuNPs. HRTEM image of AuNPs (inset) shows well-resolved crystal lattice fringes, demonstrating the highly crystalline nature of the synthesized nanoparticle. The corresponding energy dispersive X-ray analysis (EDX), as shown in Fig. 2B. The result revealed the composition was mainly C, Cu, S, Ru, and Au. Strong signals from Ru, and Au suggested the successful synthesis $Ru(bpy)_3^{2+}$/AuNPs composite. Other peaks originated from the substrate.

The as-prepared $Ru(bpy)_3^{2+}$/AuNPs colloid was further characterized by means of UV–vis spectrophotometer. Fig. 2C shows UV–vis spectra of $HAuCl_4$ (a), dilute $Ru(bpy)_3^{2+}$/AuNPs colloid (b) in deionized water. As shown in Fig. 2C(curve a), there is a strong absorption band at 290 nm that corresponds to the absorption of $AuCl_4^-$, while in the UV spectrum of $Ru(bpy)_3^{2+}$/AuNPs colloid, the absorption peaks at 290 nm disappear completely in Fig. 2C(curve b), indicating the full reduction of $HAuCl_4$. And the $Ru(bpy)_3^{2+}$/AuNPs colloid exhibited new peaks at 242 nm, 289 nm and 450 nm as that of $Ru(bpy)_3^{2+}$ solution,

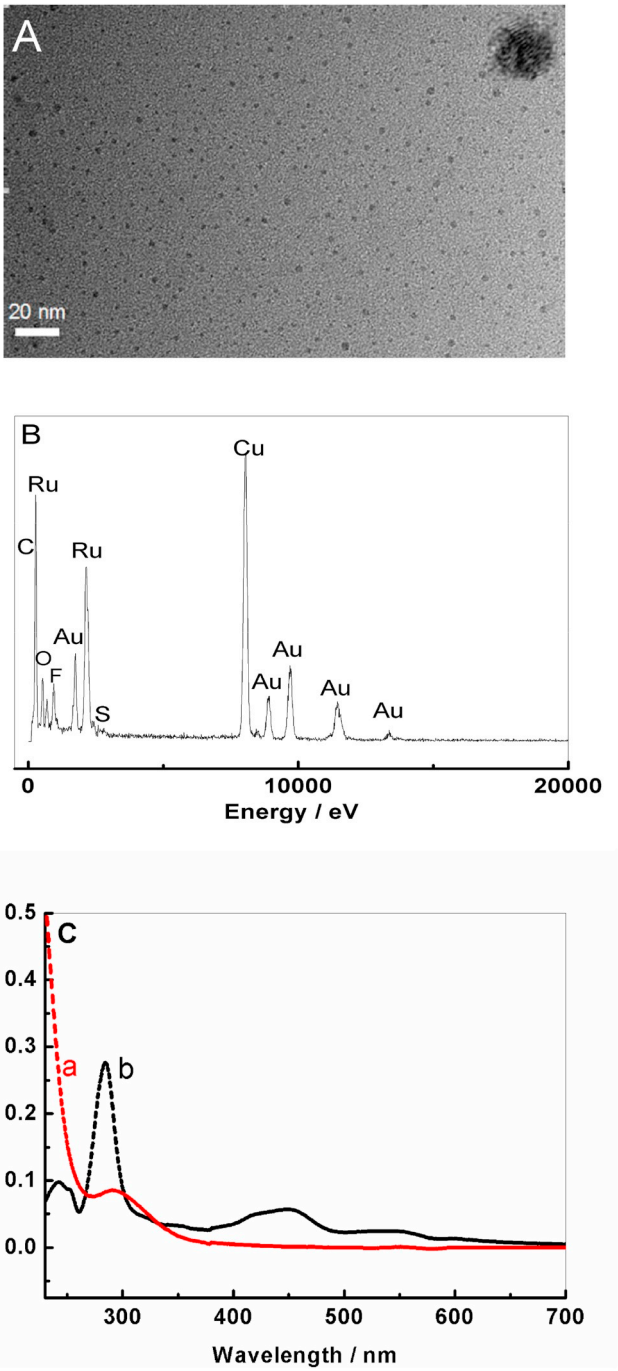

Fig. 2. TEM image(A), corresponding EDX spectrum(B) and UV–visible spectra (C) of the $Ru(bpy)_3^{2+}$/AuNPs colloid. Inset(A): HRTEM of AuNPs.

which were due to electronic π-π* transition and MLCT absorption of $Ru(bpy)_3^{2+}$ [44,45]. The above experimental results showed the preparation procedure of AuNPs had no effect on $Ru(bpy)_3^{2+}$ in the Nafion polymer.

3.3. Characterization of solid-state $Ru(bpy)_3^{2+}$ ECL film

Figure S4A shows the cyclic voltammograms (CVs) of the $Ru(bpy)_3^{2+}$/AuNPs modified Au electrode. one anodic peak at 1.15 V (P_1) and two cathodic peaks at 1.10 V (P_2) and 0.50 V (P_3) occur. Please note that the CV of bare $Ru(bpy)_3^{2+}$/nafion-modified Au electrode shows two peaks at 1.15 and 1.10 V(inset a) resulting from the oxidation and reduction of the $Ru(bpy)_3^{2+}$, respectively and the CV of bare

AuNPs/Nafion modified Au electrode also shows two peaks at 1.1 and 0.50 V (inset b) resulting from the oxidation and reduction of the AuNPs(or Au electrode), respectively. When $Ru(bpy)_3^{2+}$/AuNPs composite modified on the Au electrode, oxidation peak of $Ru(bpy)_3^{2+}$ and AuNPs overlaps, therefore, the peak P_1 can be assigned to the oxidation peak of $Ru(bpy)_3^{2+}$ and AuNPs(or Au electrode) contained in the composite, the peak P_2 can be assigned to cathodic peak of $Ru(bpy)_3^{2+}$ and the peak P_3 can be assigned to cathodic peak of AuNPs(or Au electrode). Figure S4B shows corresponding ECL intensity-potential (I_{ECL}-E) curve of the $Ru(bpy)_3^{2+}$/AuNPs modified Au electrode. On a positive scan, one anodic luminescence appeared at near 0.99 V and reached the maximum at 1.15 V, which are attributed to $Ru(bpy)_3^{2+}$ ECL. However, on a negative scan, one cathodic luminescence occurred, this is not surprising, it is attributed to cathodic ECL of AuNPs according to previous report [46]. These results showed that $Ru(bpy)_3^{2+}$/AuNPs was succesfully immobilized on the surface of Au electrode.

3.4. Characterization of stepwise fabrication of the DNA-detection protocol based on ERET

Resonance energy transfer (RET) is a process in which an excited-state donor chromophore can transfer energy to a proximal acceptor (typically < 10 nm) through a long-range nonradiative dipole-dipole coupling [47]. Much work [48–50] has revealed that the spectral overlap between emission of a donor and absorption of an acceptor enables the resonance energy transfer process. As ECL from $Ru(bpy)_3^{2+}$ film ranged from 500 nm to 800 nm [51], the absorption of the GO (Figure S1) was partly overlapped with this spectral range. So, the energy transfer from $Ru(bpy)_3^{2+}$ to GO can occur.

The fabrication process of the ERET platform was confirmed by I_{ECL}-E curves of various electrodes in 100 mM PBS containing 3.0 mM TPA(Fig. 3A). No ECL signal was obtained on a bare Au electrode (not shown). When $Ru(bpy)_3^{2+}$/AuNPs was immobilized on Au electrode, a strong ECL signal appeared(curve a). After binding to HS-DNA, the ECL of HS-ssDNA-$Ru(bpy)_3^{2+}$/AuNPs decreased for the quenching of the base(curve b), while in the presence of 0.02 mg mL^{-1} GO (curve c), ECL signal decreased sharply, only about 10% ECL is observed. Inset shows the ECL intensity-time curves under continuous scanning for six cycles. The results suggested that the film were quite stable. From the dependence of ECL intensity of HS-ssDNA-$Ru(bpy)_3^{2+}$/AuNPs on GO concentration(Fig. 3B), the ECL quenching could be described by the Stern-Volmer equation with a quenching constant of 1.6×10^5 $(g/mL)^{-1}$, indicating a dynamic quenching process [52]. The results showed that the ECL of HS-ssDNA-$Ru(bpy)_3^{2+}$/AuNPs can be efficiently quenched by GO. The decrease of the ECL intensity in the presence of GO could be attributed to the quenching reactions, including the π–π stacking interaction between the GO and the base, hydrogen bonding interaction between –OH or –COOH groups of GO and –OH or $–NH_2$ groups of HS-ssDNA, which led to the adsorption of HS-ssDNA on GO and ECL quenching through ERET.

The fabrication process of the ECL-RET platform was also confirmed by EIS, (Fig. 4A). The impedance spectrum includes a semicircle portion and a linear portion. The semicircle diameter at higher frequencies corresponds to the electron-transfer resistance (Ret), and the linear part at lower frequencies corresponds to the diffusion process. It was observed that the EIS of bare Au electrode displayed an almost straight line (curve a), which was characteristic of a diffusion process(2Ω). When $Ru(bpy)_3^{2+}$/Nafion was immobilized on the electrode, the Ret (1.26E5Ω) increased obviously, which indicated that Nafion in the film blocked electron transfer, but when $Ru(bpy)_3^{2+}$/AuNPs was assembled on the Au electrode surface, the Ret(5.6Ω) decreased obviously (curve b), which is the same like bare Au electrode, indicating that the $Ru(bpy)_3^{2+}$/AuNPs were immobilized on the electrode surface and AuNPs increased the electron-transfer efficiency. The addition of the HS-ssDNA layer resulted in a larger Ret of 34Ω (curve c), mainly due to the electrostatic repulsion between negative charges of the DNA backbone

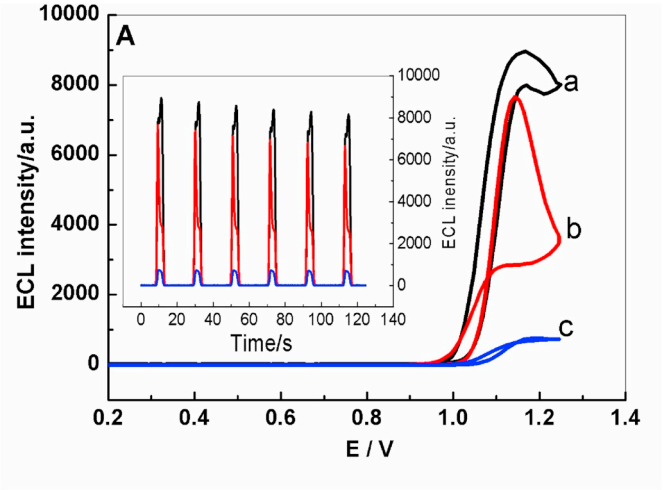

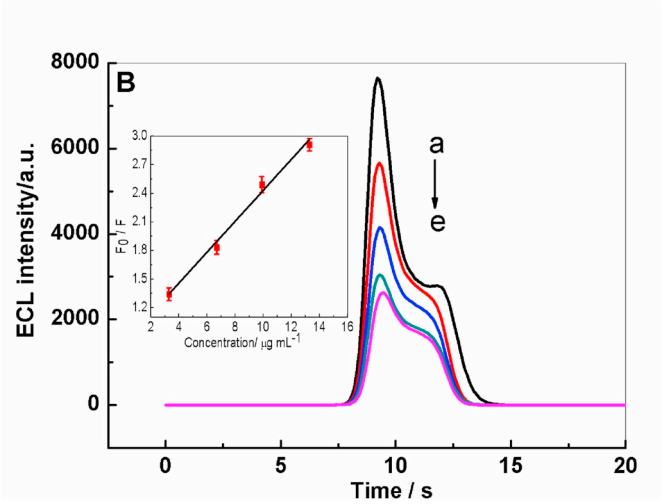

Fig. 3. ECL intensity-E curve(A) of $Ru(bpy)_3^{2+}$/AuNPs electrode(a), Ru $(bpy)_3^{2+}$/AuNPs/HS-ssDNA electrode without (b) and with 0.2 mg mL^{-1} GO (c) in 100 mM PBS (pH 7.4) containing 3 mM TPA. Inset: ECL intensity-time curves under continuous CVs for 6 cycles. Scan rate, 100 mV s^{-1}. ECL spectra of $Ru(bpy)_3^{2+}$/AuNPs–HS–ssDNA at GO concentration of 0, 3.3, 6.6, 9.9, 13.3 μg/mL(a→e) (B). **Inset**: Stern-Volmer plot for the quenching of $Ru(bpy)_3^{2+}$/AuNPs/HS-ssDNA film by GO.

and $Fe(CN)_6^{3-/4-}$, then inhibiting electron transfer. On hybridization with the target sequence, a relatively large increased Ret is observed (curve d) due to more dense and crowded negative charges of DNA.

The approach curves of different modified electrodes were recorded by using in 1 mM ferricyanide redox mediator in 0.1 M KCl and a tip potential of −0.1 V versus Ag/AgCl to generate ferrocyanide at s steady state. Fig. 4B shows the theoretical curves are fitting to the experimental data. Bare Au electrode (curve a) and $Ru(bpy)_3^{2+}$/AuNPs modified Au electrode (curve b) displayed positive feedback, which was characteristic of larger electron transfer rate constant. When HS-ssDNA layer was self-assembled on modified Au electrode (curve c) and later hybridized with t-ssDNA (curve d), negative feedback occurred, indicating electron transfer was inhibited, which was in accordance with EIS results. According to fitted values, the heterogenous rate constants (k_{eff}) were calculated. k_{eff}(a) = 0.061 cm s^{-1}, k_{eff}(b) = 0.049 cm s^{-1}, k_{eff}(c) = 0.0053 cm s^{-1} and k_{eff}(d) = 0.0036 cm s^{-1}, which indicated that HS-ssDNA had very high coverage on modified Au electrode surface.

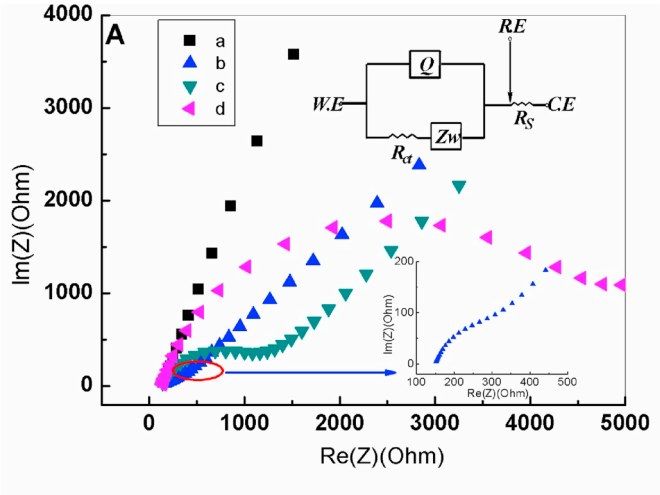

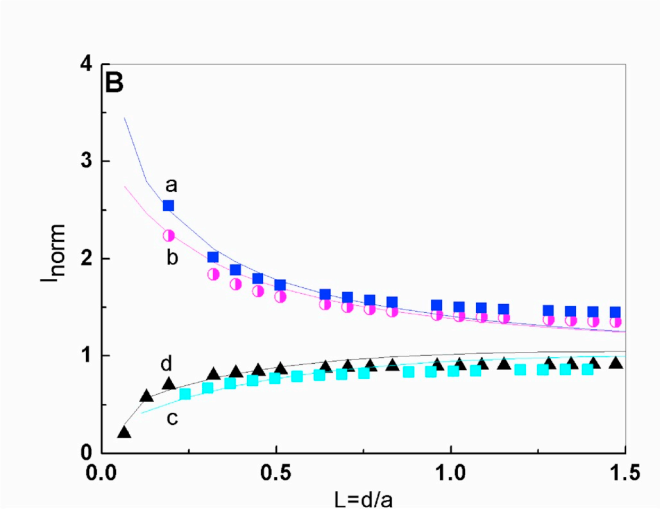

Fig. 4. EIS(A) and Probe approach curves(B) of bare Au electrode(a), Ru $(bpy)_3^{2+}$/AuNPs electrode(b), Ru$(bpy)_3^{2+}$/AuNPs/HS-ssDNA electrode(c), Ru $(bpy)_3^{2+}$/AuNPs/HS-ssDNA/t-ssDNA electrode(d) in 5.0 mM $K_3Fe(CN)_6/K_4Fe(CN)_6$. **Inset(A):** the equivalent circuit model used to obtain equations for Zre and Zim. Rs, Rct, Cdl and Zw represent the resistance of electrolyte, the charge transfer resistance, double-layer capacitance and the Warburg impedance, respectively.

3.5. ECL detection

The ECL intensity increased with the increasing concentration of t-ssDNA (Fig. 5A). The ECL intensity vs. t-ssDNA concentration showed a linear calibration in the range from 50 to 1000 pM. The limit of detection (LOD) for target DNA was 20 pM.

The specificity of the HS-ssDNA-Ru$(bpy)_3^{2+}$/AuNPs probe was studied by using four different DNA sequences, including a perfectly complementary DNA, one-base mismatched DNA, three-base mismatched DNA, or noncomplementary DNA, respectively. As shown in Fig. 5B, the HS-ssDNA-Ru$(bpy)_3^{2+}$/AuNPs probe presented good performance to discriminate the perfectly complementary target and the mismatched stand. Upon addition of 0.2 mg mL^{-1} GO, the perfectly complementary t-ssDNA showed a I_0/I value of 2.5 times that for single-base mismatch sequence (histograms 1 and 2), indicating good selectivity. The response to the three-base mismatch stand was only 15% of that for the perfectly complementary target (histogram 3), which was close to the blank control (histogram 4). These results demonstrated that the proposed approach was able to detect effectively the target with high specificity.

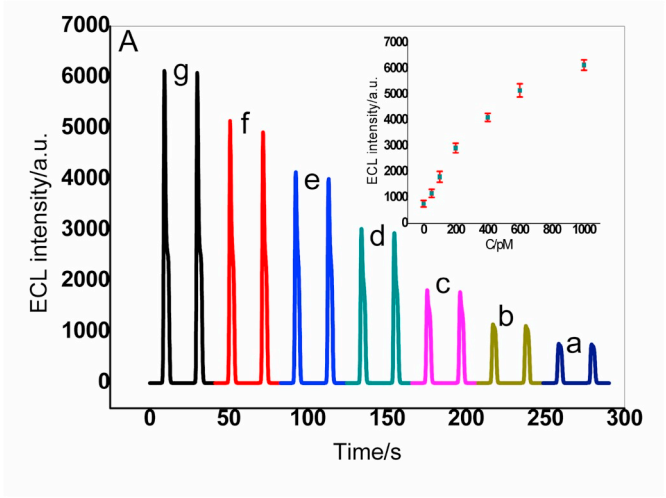

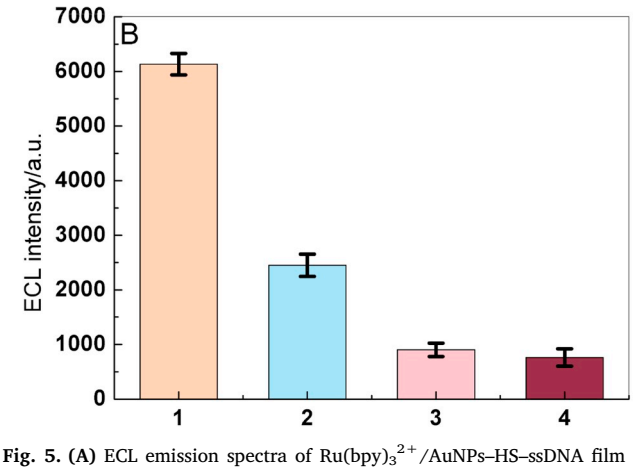

Fig. 5. (A) ECL emission spectra of Ru$(bpy)_3^{2+}$/AuNPs–HS–ssDNA film after incubation with 0, 50, 100, 200, 400, 600 and 1000 pM t-ssDNA(a–g)then addition of 0.2 mg mL^{-1} GO for 5min. Inset: The ECL intensity as a function of the t-ssDNA concentration. **(B)** ECL intensity of Ru$(bpy)_3^{2+}$/AuNPs–HS–ssDNA after incubation with 1000pM complementary DNA(1), one-base mismatch DNA(2), three-base mismatch DNA(3) and noncomplementary DNA (4) in the presence of 0.2 mg mL^{-1} GO.

4. Conclusions

In summary, we have successfully developed a novel, stable and simple solid-state ECL sensor based on ERET from Ru$(bpy)_3^{2+}$ to GO for specific detection of DNA. First, Ru$(bpy)_3^{2+}$/AuNP was successfully synthetized by a new, facile and green method. Then, DNA was marked indirectly onto the surface of electrode by preparation of Ru$(bpy)_3^{2+}$/AuNP nanocomposite materials. This solid-state ECL biosensor is lable-free with advantages such as less labor for synthesis of the Ru$(bpy)_3^{2+}$-based probe, reducing the consumption of expensive reagent et al. The GO-quenching was based on the strong ssDNA adsorption ability of GO, so GO was also not required to be labelled with DNA like other quencher(black hole, ferrocene). The label-free biosensor is very simple, fast, sensitive and selective, exhibiting a wide dynamic range from 50 nM to 1000pM with detection limit of 20pM. It is the first label-free solid-state ECL biosensor based on ERET from Ru$(bpy)_3^{2+}$ to GO.

Declaration of competing interest

The authors declare that they have no known competing financial interests or personal relationships that could have appeared to influence the work reported in this paper.

Acknowledgements

This work was supported by Scientific Research Fundation of Mianyang Normal University (QD2015A008), and Key fund Project of Sichuan Provincial Department of Education (18ZA0256).

Appendix A. Supplementary data

Supplementary data to this article can be found online at https://doi.org/10.1016/j.talanta.2020.121126.

References

[1] M. Campàs, I. Katakis, DNA biochip arraying, detection and amplification strategies, TrAC Trends Anal. Chem. (Reference Ed.) 23 (2004) 49–62.
[2] X. Su, R. Robelek, Y. Wu, G. Wang, W. Knoll, Detection of point mutation and insertion mutations in DNA using a quartz crystal microbalance and MutS, a mismatch binding protein, Anal. Chem. 76 (2003) 489–494.
[3] H.J. Parab, C. Jung, J.H. Lee, H.G. Park, A gold nanorod-based optical DNA biosensor for the diagnosis of pathogens, Biosens. Bioelectron. 26 (2010) 667–673.
[4] Y. Yu, C. Feng, A.M. Caminade, J.P. Majoral, W. Knoll, The detection of DNA hybridization on phosphorus dendrimer multilayer films by surface plasmon field enhanced-fluorescence spectroscopy, Langmuir 25 (2009) 13680–13684.
[5] Y. Xiang, Z. Wang, H. Xing, N.Y. Wong, Y. Lu, Label-free fluorescent functional DNA sensors using unmodified DNA: a vacant site approach, Anal. Chem. 82 (2010) 4122–4129.
[6] O.A. Sadik, A.O. Aluoch, A. Zhou, Status of biomolecular recognition using electrochemical techniques, Biosens. Bioelectron. 24 (2009) 2749–2765.
[7] W. Miao, A.J. Bard, Electrogenerated chemiluminescence. 77. DNA hybridization detection at high amplification with $[Ru(bpy)_3]^{2+}$-Containing microspheres, Anal. Chem. 76 (2004) 5379–5386.
[8] I.H. Franke-Whittle, S.H. Klammer, S. Mayrhofer, H. Insam, Comparison of different labeling methods for the production of labeled target DNA for microarray hybridization, J. Microbiol. Methods 65 (2006) 117–126.
[9] A.A. Gorodetsky, M.C. Buzzeo, J.K. Barton, DNA-mediated electrochemistry, Bioconjugate Chem. 19 (2008) 2285–2296.
[10] J. Han, Y. Zhuo, Y. Chai, G. Gui, M. Zhao, Q. Zhu, R. Yuan, A signal amplification strategy using the cascade catalysis of gold nanoclusters and glucose dehydrogenase for ultrasensitive detection of thrombin, Biosens. Bioelectron. 50 (2013) 161–166.
[11] W.C. Law, K.T. Yong, A. Baev, P.N. Prasad, Sensitivity improved surface plasmon resonance biosensor for cancer biomarker detection based on plasmonic enhancement, ACS Nano 5 (2011) 4858–4864.
[12] C.F. Huang, G.H. Yao, R.P. Liang, J.D. Qiu, Graphene oxide and dextran capped gold nanoparticles based surface plasmon resonance sensor for sensitive detection of concanavalin A, Biosens. Bioelectron. 50 (2013) 305–310.
[13] P. Bertoncello, R.J. Forster, Nanostructured materials for electrochemiluminescence (ECL)-based detection methods: recent advances and future perspectives, Biosens. Bioelectron. 24 (2009) 3191–3200.
[14] D.Y. Liu, Y.Y. Xin, X.W. He, X.B. Yin, The electrochemiluminescence of ruthenium complex/tripropylamine systems at DNA-modified gold electrodes, Biosens. Bioelectron. 26 (2011) 2703–2706.
[15] G. Gui, Y. Zhuo, Y.Q. Chai, N. Liao, M. Zhao, J. Han, Q. Zhu, R. Yuan, Y. Xiang, Supersandwich-type electrochemiluminescenct aptasensor based on $Ru(phen)_3^{2+}$ functionalized hollow gold nanoparticles as signal-amplifying tags, Biosens. Bioelectron. 47 (2013) 524–529.
[16] J. Wang, W.W. Zhao, H. Zhou, J.J. Xu, H.Y. Chen, Amplified electrochemiluminescence detection of DNA-binding protein based on the synergy effect of electron and energy transfer between CdS nanocrystals and gold nanoparticles, Biosens. Bioelectron. 41 (2013) 615–620.
[17] W. Miao, J.P. Choi, A.J. Bard, Electrogenerated chemiluminescence 69: the tris(2,2‘-bipyridine)ruthenium(II), ($Ru(bpy)_3^{2+}$)/Tri-n-propylamine (TPrA) system RevisitedA new route involving TPrA•+ cation radicals, J. Am. Chem. Soc. 124 (2002) 14478–14485.
[18] A.W. Knight, A review of recent trends in analytical applications of electrogenerated chemiluminescence, TrAC Trends Anal. Chem. (Reference Ed.) 18 (1999) 47–62.
[19] W. Miao, Electrogenerated chemiluminescence and its biorelated applications, Chem. Rev. 108 (2008) 2506–2553.
[20] L. Hu, G. Xu, Applications and trends in electrochemiluminescence, Chem. Soc. Rev. 39 (2010) 3275–3304.
[21] M. Su, W. Wei, S. Liu, Analytical applications of the electrochemiluminescence of tris(2,2′-bipyridyl)ruthenium(II) coupled to capillary/microchip electrophoresis: a review, Anal. Chim. Acta 704 (2011) 16–32.
[22] H. Wei, E. Wang, Electrochemiluminescence of tris(2,2′-bipyridyl)ruthenium and its applications in bioanalysis: a review, Luminescence 26 (2011) 77–85.
[23] J. Li, E. Wang, Applications of tris(2,2′-bipyridyl)ruthenium(II) in electrochemiluminescence, Chem. Rec. 12 (2012) 177–187.
[24] H. Wei, E. Wang, Solid-state electrochemiluminescence of tris(2,2′-bipyridyl) ruthenium, TrAC Trends Anal. Chem. (Reference Ed.) 27 (2008) 447–459.
[25] Y. Du, B. Qi, X. Yang, E. Wang, Synthesis of PtNPs/AQ/$Ru(bpy)_3^{2+}$ colloid and its application as a sensitive solid-state electrochemiluminescence sensor material, J. Phys. Chem. B 110 (2006) 21662–21666.
[26] X. Sun, Y. Du, L. Zhang, S. Dong, E. Wang, Pt Nanoparticles: heat treatment-based preparation and $Ru(bpy)_3^{2+}$-Mediated formation of aggregates that can form stable films on bare solid electrode surfaces for solid-state electrochemiluminescence detection, Anal. Chem. 78 (2006) 6674–6677.
[27] X. Sun, Y. Du, S. Dong, E. Wang, Method for effective immobilization of $Ru(bpy)_3^{2+}$ on an electrode surface for solid-state electrochemiluminescene detection, Anal. Chem. 77 (2005) 8166–8169.
[28] Y. Liao, R. Yuan, Y. Chai, L. Mao, Y. Zhuo, Y. Yuan, L. Bai, S. Yuan, Electrochemiluminescence quenching via capture of ferrocene-labeled ligand-bound aptamer molecular beacon for ultrasensitive detection of thrombin, Sens. Actuators, B 158 (2011) 393–399.
[29] X. Wang, P. Dong, W. Yun, Y. Xu, P. He, Y. Fang, A solid-state electrochemiluminescence biosensing switch for detection of thrombin based on ferrocene-labeled molecular beacon aptamer, Biosens. Bioelectron. 24 (2009) 3288–3292.
[30] X. Wang, W. Yun, P. Dong, J. Zhou, P. He, Y. Fang, A controllable solid-state $Ru(bpy)_3^{2+}$ electrochemiluminescence film based on conformation change of ferrocene-labeled DNA molecular beacon, Langmuir 24 (2008) 2200–2205.
[31] W. Gao, X.H. Xia, J.J. Xu, H.Y. Chen, Three-dimensionally ordered macroporous gold structure as an efficient matrix for solid-state electrochemiluminescence of $Ru(bpy)_3^{2+}$/TPA system with high sensitivity, J. Phys. Chem. C 111 (2007) 12213–12219.
[32] L.J. Cote, R. Cruz-Silva, J. Huang, Flash reduction and patterning of graphite oxide and its polymer composite, J. Am. Chem. Soc. 131 (2009) 11027–11032.
[33] Z. Liu, J.T. Robinson, X. Sun, H. Dai, PEGylated nanographene oxide for delivery of water-insoluble cancer drugs, J. Am. Chem. Soc. 130 (2008) 10876–10877.
[34] C.H. Lu, H.H. Yang, C.L. Zhu, X. Chen, G.N. Chen, A graphene platform for sensing biomolecules, Angew. Chem. Int. Ed. 48 (2009) 4785–4787.
[35] N. Varghese, U. Mogera, A. Govindaraj, A. Das, P.K. Maiti, A.K. Sood, C.N.R. Rao, Binding of DNA nucleobases and nucleosides with graphene, ChemPhysChem 10 (2009) 206–210.
[36] C.H. Lu, J. Li, J.J. Liu, H.H. Yang, X. Chen, G.N. Chen, Increasing the sensitivity and single-base mismatch selectivity of the molecular beacon using graphene oxide as the “nanoquencher”, Chem. Eur J. 16 (2010) 4889–4894.
[37] H. Dong, W. Gao, F. Yan, H. Ji, H. Ju, Fluorescence resonance energy transfer between quantum dots and graphene oxide for sensing biomolecules, Anal. Chem. 82 (2010) 5511–5517.
[38] W. Wei, D.F. Li, X.H. Pan, S.Q. Liu, Electrochemiluminescent detection of Mucin 1 protein and MCF-7 cancer cells based on the resonance energy transfer, Analyst 137 (2012) 2101–2106.
[39] W.S. Hummers, R.E. Offeman, Preparation of graphitic oxide, J. Am. Chem. Soc. 80 (1958) 1339-1339.
[40] S. Stankovich, D.A. Dikin, G.H.B. Dommett, K.M. Kohlhaas, E.J. Zimney, E.A. Stach, R.D. Piner, S.B.T. Nguyen, R.S. Ruoff, Graphene-based composite materials, Nature 442 (2006) 282–286.
[41] N. Mohanty, V. Berry, Graphene-based single-bacterium resolution biodevice and DNA transistor: interfacing graphene derivatives with nanoscale and microscale biocomponents, Nano Lett. 8 (2008) 4469–4476.
[42] S. Stankovich, D.A. Dikin, R.D. Piner, K.A. Kohlhaas, A. Kleinhammes, Y. Jia, Y. Wu, S.B.T. Nguyen, R.S. Ruoff, Synthesis of graphene-based nanosheets via chemical reduction of exfoliated graphite oxide, Carbon 45 (2007) 1558–1565.
[43] Y. Si, E.T. Samulski, Synthesis of water soluble graphene, Nano Lett. 8 (2008) 1679–1682.
[44] Z. Guo, Y. Shen, M. Wang, F. Zhao, S. Dong, Electrochemistry and electrogenerated chemiluminescence of SiO_2 nanoparticles/tris(2,2‘-bipyridyl)ruthenium(??) multilayer films on indium tin oxide electrodes, Anal. Chem. 76 (2003) 184–191.
[45] W. Miao, A.J. Bard, Electrogenerated chemiluminescence. 72. Determination of immobilized DNA and C-reactive protein on Au(111) electrodes using tris(2,2‘-bipyridyl)ruthenium(II) labels, Anal. Chem. 75 (2003) 5825–5834.
[46] X. Lu, D. liu, J. Du, H. Wang, Z. Xue, X. Liu, X. Zhou, Novel cathodic electrochemiluminescence of tris(bipyridine) ruthenium(ii) on a gold electrode in acidic solution, Analyst 137 (2012) 588–594.
[47] S. Ge, J. Lu, M. Yan, F. Yu, J. Yu, X. Sun, Fluorescence resonance energy transfer sensor between quantum dot donors and neutral red acceptors and its detection of BSA in micelles, Dyes Pigments 91 (2011) 304–308.
[48] Y. Shan, J.J. Xu, H.Y. Chen, Electrochemiluminescence quenching by CdTe quantum dots through energy scavenging for ultrasensitive detection of antigen, Chem. Commun. 46 (2010) 5079–5081.
[49] Y. Shan, J.J. Xu, H.Y. Chen, Distance-dependent quenching and enhancing of electrochemiluminescence from a CdS:Mn nanocrystal film by Au nanoparticles for highly sensitive detection of DNA, Chem. Commun. (2009) 905–907.
[50] G. Jie, B. Liu, H. Pan, J.-J. Zhu, H.Y. Chen, CdS nanocrystal-based electrochemiluminescence biosensor for the detection of low-density lipoprotein by increasing sensitivity with gold nanoparticle amplification, Anal. Chem. 79 (2007) 5574–5581.
[51] Y.Q. Pang, H. Cui, H.-S. Zheng, G.H. Wan, L.J. Liu, X.F. Yu, Flow injection analysis of tetracyclines using inhibited $Ru(bpy)_3^{2+}$/tripropylamine electrochemiluminescence system, Luminescence 20 (2005) 8–15.
[52] B. Huang, X. Zhou, Z. Xue, G. Wu, J. Du, D. Luo, T. Liu, J. Ru, X. Lu, Quenching of the electrochemiluminescence of $Ru(bpy)_3^{2+}$/TPA by malachite green and crystal violet, Talanta 106 (2013) 174–180.